

# Vacuum Birefringence, Ellipticity, and the Anomalous Magnetic Moment of a Photon

S. R. Valluri

*Department of Physics and Astronomy and Department of Mathematics, The University of Western Ontario,  
and King's University College (UWO) London Ontario N6A 3K7 Canada\**

F. A. Chishtie

*Peaceful Society, Science and Innovation Foundation,  
Vancouver, British Columbia V6K 2E4 Canada and  
Department of Occupational Science and Occupational Therapy,  
The University of British Columbia, Vancouver British Columbia V6T 2L4 Canada†*

J. W. Mielniczuk‡

*82 Brick Kiln Road Apt 1-301, Chelmsford, MA 01824, USA*

(Dated: March 10, 2026)

We study photon propagation in a strong magnetic field  $B \sim B_{\text{cr}}$ , where  $B_{\text{cr}} = \frac{m_e^2}{e} \simeq 4.4 \times 10^{13}$  Gauss is the Schwinger critical field. We show that the expected value of the Hamiltonian of a quantized photon for a perpendicular mode is a convex function of the magnetic field  $B$ . We find that the anomalous magnetic moment of a photon in the one-loop approximation is a non-decreasing function of the magnetic field  $B$  in the range  $0 \leq B \leq 30 B_{\text{cr}}$ . We find that the anomalous magnetic moment  $\mu_\gamma$  of a photon for  $B = 30 B_{\text{cr}}$  is  $\sim 8/3$  of the anomalous magnetic moment of a photon for  $B = 1/2 B_{\text{cr}}$ . We establish new connections between  $\mu_\gamma$ , vacuum birefringence, and directly measurable polarization observables. Based on recent experimental observations—including the ATLAS detection of light-by-light scattering at  $8.2\sigma$  significance, IXPE X-ray polarimetry of magnetars revealing polarization degrees up to 80%, and continuing PVLAS measurements approaching QED sensitivity—we provide predictions for ellipticity and polarization degree as important observables for future experiments. Numerical verification of our analytical results confirms the theoretical predictions with high precision.

## I. INTRODUCTION

The nonlinearity of Maxwell's equations in the quantum regime continues to present us with a variety of fascinating phenomena. Born and Infeld (1934) pioneered nonlinear electrodynamics from the perspective of classical field theory [12, 24]. The effective interaction resulting from corrections due to virtual excitations of charged quantum fields, such as electron  $e^-$  and positron  $e^+$ , leads to well-known interesting effects [5, 21]. More recently, other aspects of the quantum vacuum have been explored by Shabad & Usov [65], Villalba-Chávez & Shabad [76], and Altschul [2], to name but a few.

In the case of electromagnetic fields that vary slowly with respect to the Compton wavelength, i.e., frequencies much less than the pair creation threshold, the one-loop quantum electrodynamic effective Heisenberg-Euler Lagrangian (HEL) [22, 35, 50, 65, 76] describes the dominant physical effects. The HEL is known to all orders in electromagnetic fields. It is well established that electrons acquire an anomalous magnetic moment due to radiative corrections in quantum electrodynamics (QED)

with  $e^- - e^+$  pairs and virtual photons in the background [64]. It is also of fundamental interest that there exists an anomalous photon magnetic moment  $\mu_\gamma$  due to interaction with external magnetic fields in the environment of virtual  $e^- - e^+$  quanta of the vacuum.

The last few decades have seen a resurgence of interest in quantum vacuum physics [6, 7, 23, 28, 37–39, 52]. The analytical proof that higher harmonics arise from the nonlinear HEL in the ultra-strong field limit was given by Bhartia & Valluri [53] and subsequently extended to the weak-field case by Valluri & Bhartia [54]; these foundational results establish the harmonic structure of the QED vacuum that motivates the present analysis. The promise of high-intensity experimental facilities ( $\sim 10^{15}$  W) has stimulated immense interest in investigating the nonlinear quantum vacuum in practical optical experiments [17, 18, 23, 49]. The Polarization of the Vacuum with Laser (PVLAS) experiment aims to measure the birefringence of vacuum in an external magnetic field [13, 15, 19, 26, 81]. After 25 years of dedicated effort, PVLAS has achieved sensitivities approaching the QED prediction, with current limits of  $\Delta n = (12 \pm 17) \times 10^{-23}$  at  $B = 2.5$  T [26], now within a factor of 5 of the QED prediction  $\Delta n_{\text{QED}} \simeq 2.5 \times 10^{-23}$ .

Magnetars such as SGR 1806-20, with magnetic fields of order  $10^{15}$  Gauss, are of particular interest for our work [42]. Direct evidence of vacuum birefringence via optical polarimetry has been reported by Mignani et al. (2017) [55], who studied the radio-quiet neutron star RX

\* valluri@uwo.ca

† fachisht@uwo.ca

‡ Deceased, July 2016. Dr. Mielniczuk contributed to the analytical derivations in Appendices A–C and the numerical verification of monotonicity proofs before his passing.

J1856.5-3754; we have examined further astrophysical implications of their findings in Ref. [73].

Most recently, dramatic experimental progress has been achieved on multiple fronts. The ATLAS collaboration at the Large Hadron Collider observed light-by-light scattering in ultra-peripheral heavy-ion collisions with a significance of  $8.2\sigma$  [3, 4], with a measured cross-section  $\sigma = 78 \pm 15$  nb in excellent agreement with the QED prediction of  $\sim 70$  nb, directly confirming the nonlinear photon-photon interaction predicted by QED. NASA's Imaging X-ray Polarimetry Explorer (IXPE) has detected polarized X-rays from magnetars with polarization degrees reaching 65–80% [43, 44, 46, 67], providing compelling evidence for vacuum birefringence effects in ultra-strong magnetic fields. These observations, together with the “photon mode conversion” phenomenon at the QED vacuum resonance [46], open exciting possibilities for testing nonlinear QED through astrophysical sources.

The photon anomalous magnetic moment and its paramagnetic properties have been studied by Pérez Rojas & Rodríguez Quets [59, 62, 63], who provided values of  $\mu_\gamma$  in the two extreme limits  $B \ll B_{\text{cr}}$  and  $B \gg B_{\text{cr}}$ . The purpose of this paper is to provide numerical values and analytic formulas for the intermediate range  $B \sim B_{\text{cr}}$ , and to establish explicit connections between  $\mu_\gamma$  and experimentally measurable quantities. Our results are applicable in the range  $0 \leq B \leq 30 B_{\text{cr}}$ .

The paper is organized as follows. In Section II, we establish the theoretical framework and define all relevant quantities, including the polarization modes and the angle  $\theta$  between  $\mathbf{B}$  and  $\mathbf{k}$ . In Section V, we derive the anomalous magnetic moment of the photon with complete analytical results. In Section VI, we connect  $\mu_\gamma$  to measurable birefringence and ellipticity observables. In Section VII, we outline the photon center of mass and group velocity. In Section VIII, we present experimental comparisons and predictions, including detailed numerical verification of our theoretical results. Section IX contains our conclusions. Supplementary mathematical details are provided in Appendices A, B, and C.

## II. THEORETICAL FRAMEWORK

### A. Heisenberg-Euler Effective Lagrangian

At one-loop order, the Heisenberg-Euler effective Lagrangian in constant external electromagnetic fields [35, 45], describing effective nonlinear interactions between electromagnetic fields mediated by electron-positron fluctuations in the vacuum, can be represented in terms of the proper-time integral [64]:

$$\mathcal{L} = \frac{\alpha}{2\pi} \int_0^\infty \frac{ds}{s} e^{-i\frac{m^2}{e}s} \left[ ab \coth(as) \cot(bs) - \frac{a^2 - b^2}{3} - \frac{1}{s^2} \right] \quad (1)$$

with the prescription  $m^2 \rightarrow m^2 - i0^+$ , and the proper-time integration contour assumed to lie slightly below the real positive  $s$  axis. Here,  $m$  is the electron mass,  $e$  is the elementary charge,  $\alpha = \frac{e^2}{4\pi}$  is the fine structure constant, and

$$a = \left( \sqrt{\mathcal{F}^2 + \mathcal{G}^2} - \mathcal{F} \right)^{1/2}, \quad (2)$$

$$b = \left( \sqrt{\mathcal{F}^2 + \mathcal{G}^2} + \mathcal{F} \right)^{1/2} \quad (3)$$

are the secular invariants constructed from the gauge and Lorentz invariants of the electromagnetic field:

$$\mathcal{F} = \frac{1}{4} F_{\mu\nu} F^{\mu\nu} = \frac{1}{2} (\mathbf{B}^2 - \mathbf{E}^2), \quad (4)$$

$$\mathcal{G} = \frac{1}{4} F_{\mu\nu}^* F^{\mu\nu} = -\mathbf{E} \cdot \mathbf{B}, \quad (5)$$

with  $F^{*\mu\nu} = \frac{1}{2} \epsilon^{\mu\nu\alpha\beta} F_{\alpha\beta}$  denoting the dual field strength tensor;  $\epsilon^{\mu\nu\alpha\beta}$  is the totally antisymmetric tensor with  $\epsilon^{0123} = 1$ . Our metric convention is  $g_{\mu\nu} = \text{diag}(-1, +1, +1, +1)$ , and we use units where  $c = \hbar = 1$ .

The seminal paper of Schwinger [64] on gauge invariance and vacuum polarization employed the proper-time parameter formulation to solve the equation of motion of a particle, yielding an effective Lagrangian [45] that is finite, gauge invariant, and Lorentz invariant. The derivative expansion of the one-loop effective Lagrangian in QED has been studied by Gusynin & Shovkovy [30]. Their non-perturbative term is that derived by Schwinger, while the second term in their expansion shows explicitly the two derivatives of  $F_{\mu\nu}$  that account for slowly or rapidly varying fields. We do not consider these derivative corrections here, working in the constant-field approximation, but note that additional terms warrant further study.

The two-loop Heisenberg-Euler effective action, including a previously overlooked finite one-particle-reducible contribution in constant fields, has been worked out by Gies & Karbstein [31]; for the weak-field regime of interest to laboratory experiments, the two-loop correction amounts to a  $\lesssim 1\%$  effect on vacuum birefringence [31]. Numerical simulation of the leading weak-field Heisenberg-Euler corrections, including up to six-photon interactions, is now available through the open-source HEWES code [32], which provides important support for analytical predictions such as those developed here.

If the typical frequency/momentum scale of variation of the background field is  $\nu$ , derivatives effectively translate into multiplications with  $\nu$ , to be rendered dimensionless by the electron mass  $m$ . Thus, Eq. (1) is also applicable for slowly varying inhomogeneous fields satisfying  $\nu/m \ll 1$ , i.e., for inhomogeneities whose typical spatial (temporal) scales of variation are much larger than the Compton wavelength (time)  $\sim 1/m$  of the virtual charged particle. The electron Compton wavelength is  $\lambda_c = 3.86 \times 10^{-13}$  m and the Compton time is  $\tau_c = 1.29 \times 10^{-21}$  s. Many electromagnetic fields available in the laboratory, e.g., pulses generated by optical

high-intensity lasers [23] featuring wavelengths of  $\mathcal{O}(\mu\text{m})$  and pulse durations of  $\mathcal{O}(\text{fs})$ , are compatible with this requirement.

### B. Definition of Polarization Modes and the Angle $\theta$

We consider a photon with wave vector  $\mathbf{k}$  propagating through a region with constant magnetic field  $\mathbf{B}$  and zero electric field ( $\mathbf{E} = 0$ ), so that  $\mathcal{G} = 0$  and  $\mathcal{F} = B^2/2$ .

**Definition:** The angle  $\theta$  is defined as the angle between the external magnetic field  $\mathbf{B}$  and the photon wave vector  $\mathbf{k}$ :

$$\cos \theta = \frac{\mathbf{B} \cdot \mathbf{k}}{|\mathbf{B}||\mathbf{k}|}. \quad (6)$$

**Polarization modes:** The photon polarization state is characterized by the orientation of its electromagnetic field relative to the plane containing  $\mathbf{B}$  and  $\mathbf{k}$ :

- **Perpendicular mode ( $\perp$ ):** The photon's magnetic field  $\mathbf{B}_\gamma$  lies in the  $(\mathbf{B}, \mathbf{k})$  plane. Equivalently, the photon's electric field  $\mathbf{E}_\gamma$  is perpendicular to this plane.
- **Parallel mode ( $\parallel$ ):** The photon's electric field  $\mathbf{E}_\gamma$  lies in the  $(\mathbf{B}, \mathbf{k})$  plane.

These two modes experience different refractive indices due to vacuum birefringence, analogous to ordinary and extraordinary rays in a birefringent crystal. The vacuum acts as an anisotropic medium due to the symmetry breaking introduced by the preferred direction of  $\mathbf{B}$ .

### C. Derivatives of the Effective Lagrangian

In the absence of an external electric field, the partial derivatives of the effective action in the one-loop approximation are [47, 48]:

$$\gamma_{\mathcal{F}} = \frac{\partial \mathcal{L}}{\partial \mathcal{F}}, \quad \gamma_{\mathcal{F}\mathcal{F}} = \frac{\partial^2 \mathcal{L}}{\partial \mathcal{F}^2}, \quad \gamma_{\mathcal{G}\mathcal{G}} = \frac{\partial^2 \mathcal{L}}{\partial \mathcal{G}^2}, \quad (7)$$

all evaluated at  $\mathcal{F} = B^2/2$  and  $\mathcal{G} = 0$ . Quantities such as  $\gamma_{\mathcal{G}}$  and  $\gamma_{\mathcal{F}\mathcal{G}}$  vanish for zero electric field.

Introducing the dimensionless parameter

$$h = \frac{1}{2} \frac{B_{\text{cr}}}{B}, \quad (8)$$

where  $B_{\text{cr}} = m^2/e \simeq 4.414 \times 10^9$  T  $\simeq 4.414 \times 10^{13}$  Gauss is the Schwinger critical field, we obtain:

$$\gamma_{\mathcal{F}} = -1 - \frac{\alpha}{2\pi} \left[ \frac{1}{3} + 2h^2 - 8\zeta'(-1, h) + 4h \ln \Gamma(h) - 2h \ln h + \frac{2}{3} \ln h - 2h \ln 2\pi \right], \quad (9)$$

$$\gamma_{\mathcal{F}\mathcal{F}} = \frac{\alpha}{2\pi B^2} \left[ \frac{2}{3} + 4h^2 \psi(1+h) - 2h - 4h^2 - 4h \ln \Gamma(h) + 2h \ln 2\pi - 2h \ln h \right], \quad (10)$$

$$\gamma_{\mathcal{G}\mathcal{G}} = \frac{\alpha}{2\pi B^2} \left[ \frac{1}{3} \left( \frac{1}{h} - 1 \right) - \frac{2}{3} \psi(1+h) - 2h^2 + 8\zeta'(-1, h) - 4h \ln \Gamma(h) + 2h \ln(2\pi h) \right], \quad (11)$$

where  $\psi(x) = \Gamma'(x)/\Gamma(x)$  is the digamma function,  $\Gamma(x)$  is the gamma function, and

$$\zeta'(s, h) = \partial_s \zeta(s, h), \quad (12)$$

with  $\zeta(s, h)$  the Hurwitz zeta function. For  $s = -1$  and  $h \gg 1$  [1, 20]:

$$\zeta'(-1, h) \simeq \frac{1}{12} - \frac{h^2}{4} + \frac{\ln h}{2} \left( h^2 - h + \frac{1}{6} \right) + \int_0^\infty \frac{e^{-hx}}{x^2} \left( \frac{1}{1-e^{-x}} - \frac{1}{x} - \frac{1}{2} - \frac{x}{12} \right) dx, \quad (13)$$

for  $\text{Re}(h) > 0$ , which can be approximated as

$$\zeta'(-1, h) \simeq \frac{1}{12} - \frac{h^2}{4} + \frac{\ln h}{2} B_2(h) + \frac{1}{720h^2}, \quad (14)$$

where  $B_2(h) = h^2 - h + \frac{1}{6}$  is the second Bernoulli polynomial [57]. The integral in Eq. (13) is convergent [1].

**Remark on  $\gamma_s$ :** We define  $\gamma_s = 1 - \gamma_{\mathcal{F}}$ . From Eq. (9),  $\gamma_{\mathcal{F}} = -1 + \mathcal{O}(\alpha)$ , giving  $\gamma_s = 2 + \mathcal{O}(\alpha)$ . For consistency in the one-loop approximation where we retain only terms to  $\mathcal{O}(\alpha)$ , we use  $\gamma_s \approx 1$  in expressions that already carry a factor of  $\alpha$ . This approximation is valid for  $B \leq 30 B_{\text{cr}}$ ; radiative corrections become significant only for  $B \geq 430 B_{\text{cr}}$ , where higher-loop contributions to the effective Lagrangian must be included.

## III. REFRACTIVE INDICES AND BIREFRINGENCE

The refractive indices for perpendicular and parallel polarized photons are central to our analysis. It is useful to note that

$$\frac{4\pi}{\alpha} (n_{\perp} - 1) = \frac{2\pi B^2}{\alpha} \gamma_{\mathcal{G}\mathcal{G}}, \quad (15)$$

where  $\gamma_{\mathcal{G}\mathcal{G}}$  is defined in Eq. (11).

### A. Weak-Field Regime

For the weak-field case with  $\xi = B/B_{\text{cr}} = 1/(2h) < 1$ , the refractive index for perpendicular polarization is [37–

39]:

$$n_{\perp} = 1 + \frac{\alpha}{4\pi} \sin^2 \theta \left[ \frac{14}{45} \xi^2 - \frac{1}{3} \sum_{j=2}^{\infty} \frac{2^{2j}(6B_{2(j+1)} - (2j+1)B_{2j})}{j(2j+1)} \xi^{2j} \right] + \mathcal{O} \left[ \left( \frac{\alpha}{2\pi} \right)^2 \right], \quad (16)$$

where  $B_{2j}$  are Bernoulli numbers.

### B. Strong-Field Regime

In the strong-field limit ( $\xi > 0.5$ ):

$$n_{\perp} = 1 + \frac{\alpha}{4\pi} \sin^2 \theta \left[ \frac{2}{3} \xi - \left( 8 \ln A - \frac{1}{3} - \frac{2}{3} \gamma_E \right) - \left( \ln \pi + \frac{\pi^2}{18} - 2 - \ln \xi \right) \xi^{-1} - \left( -\frac{1}{2} - \frac{1}{6} \zeta(3) \right) \xi^{-2} - \sum_{j=3}^{\infty} \frac{(-1)^{j-1}}{2^{j-2}} \left[ \frac{j-2}{j(j-1)} \zeta(j-1) + \frac{1}{6} \zeta(j+1) \right] \xi^{-j} \right] + \mathcal{O} \left[ \left( \frac{\alpha}{2\pi} \right)^2 \right], \quad (17)$$

where  $\gamma_E \simeq 0.5772$  is the Euler-Mascheroni constant,  $A \simeq 1.28242712$  is the Glaisher-Kinkelin constant [57], and  $\zeta(3) \simeq 1.202$  is the Riemann zeta function.

Using the identity

$$\sum_{j=3}^{\infty} \frac{(-1)^{j-1}}{2^{j-2}} \left[ \frac{j-2}{j(j-1)} \zeta(j-1) + \frac{1}{6} \zeta(j+1) \right] \xi^{-j} = \frac{1}{18\xi^2} \left[ 3\xi^2 \left( 24 - 72 \ln A + 4\gamma_E + \ln \frac{4}{\pi^6} + \zeta(3) \right) + 12\xi^2 \psi \left( 1 + \frac{1}{2\xi} \right) - \pi^2 \xi \right], \quad (18)$$

we can write Eq. (17) in closed form.

For parallel polarization, the refractive index is given by [68]:

$$n_{\parallel} = 1 + \frac{\alpha}{4\pi} \sin^2 \theta \left[ -\frac{1}{3} - \frac{2}{3} \psi(1+h) + 8\zeta'(-1, h) - 2h^2 + \frac{1}{3h} - 4h \ln \Gamma(h) + 2h \ln(2\pi h) \right], \quad (19)$$

which is valid for all  $B \leq (\pi/\alpha)B_{\text{cr}}$ . The combined effect of a strong magnetic field and a weaker co-aligned electric field on vacuum birefringence, including rotation of the polarization vectors, has been analyzed by Kim & Kim [69], whose closed-form one-loop effective Lagrangian for

the combined electromagnetic wrench provides a useful generalization of our purely magnetic results.

**Domain overlap:** The weak-field expansion Eq. (16) and strong-field expansion Eq. (17) have overlapping domains of validity for  $1/2 < B/B_{\text{cr}} < 1$ . We have verified numerically that both expressions agree to within 0.1% throughout this overlap region, confirming the consistency of our analytical results.

### C. Birefringence

The vacuum magnetic birefringence is characterized by:

$$\begin{aligned} \Delta n_{\perp, \parallel} &= n_{\perp} - n_{\parallel} \\ &= \frac{\alpha \sin^2 \theta}{360\pi h^2} \left[ 20h^2 \{ 18(\ln A - 1) + h(27h + \pi^2 + 18) \} + 10h^2 \{ -6 \ln h + 18h((1-2h) \ln h - \ln(4\pi^2 h) + 2\Gamma(h)) + \ln(\pi^9/8) \} - 1 \right]. \end{aligned} \quad (20)$$

In the weak-field limit, this simplifies to the Cotton-Mouton form:

$$\Delta n = k_{\text{CM}} B^2 \sin^2 \theta, \quad (21)$$

where the QED Cotton-Mouton coefficient is

$$k_{\text{CM}} = \frac{\alpha}{15\pi} \frac{1}{B_{\text{cr}}^2} \simeq 4.0 \times 10^{-24} \text{ T}^{-2}. \quad (22)$$

### IV. ELLIPTICITY

An important physical observable related to  $\Delta n_{\perp, \parallel}$  is the ellipticity  $\chi$ , defined as

$$\chi = \frac{1}{2} k (n_{\perp} - n_{\parallel}) \ell = \frac{\pi}{\lambda} \Delta n \ell, \quad (23)$$

where  $k = |\mathbf{k}| = 2\pi/\lambda$  is the magnitude of the photon wave vector,  $\lambda$  is the wavelength, and  $\ell$  is the path length of the photon in the magnetic field region. The ellipticity can in principle be observable for appreciable values of  $k$  and  $\ell$ .

As a rough estimate, the ellipticity of a radio wave of a few hundred MHz traversing a path length of around one hundred meters can be of order a few radians or more for strong magnetic fields around a neutron star.

For the weak-field limit ( $B \ll B_{\text{cr}}$ ):

$$\chi \simeq \frac{\alpha}{15\pi} \left( \frac{B}{B_{\text{cr}}} \right)^2 \frac{\omega \ell}{c} \sin^2 \theta. \quad (24)$$

**Connection to PVLAS:** The PVLAS experiment measures ellipticity at  $B \sim 2.5$  T with optical wavelengths  $\lambda \sim 1064$  nm and effective path lengths  $\ell_{\text{eff}} \sim$

36 km (due to Fabry-Pérot cavity enhancement with  $\sim 44000$  passes). The QED prediction gives  $\chi_{\text{QED}} \sim 2.65 \times 10^{-12}$  rad, corresponding to  $\Delta n_{\text{QED}} \simeq 2.5 \times 10^{-23}$ . The current PVLAS measurement [26] of  $\Delta n = (12 \pm 17) \times 10^{-23}$  is now within a factor of approximately 5 of the QED prediction, representing remarkable experimental progress.

We illustrate the behavior of the ellipticity with respect to  $h$  in Fig. 1.

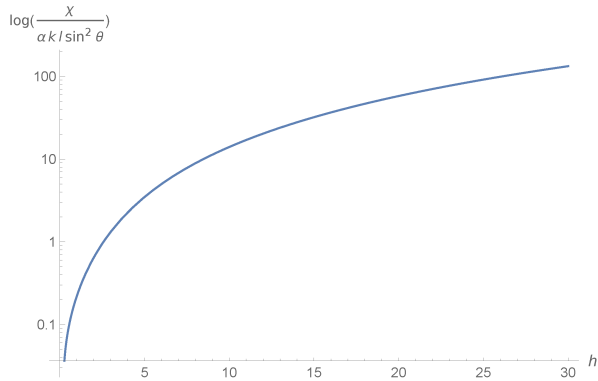


FIG. 1. Ellipticity  $\chi/(\alpha|\mathbf{k}|\ell \sin^2 \theta)$  as a function of  $h = B_{\text{cr}}/(2B)$ . The rapid growth at small  $h$  (strong-field regime) reflects the logarithmic structure of the Heisenberg-Euler Lagrangian.

## V. ANOMALOUS MAGNETIC MOMENT OF A PHOTON

### A. Hamiltonian and Definition of $\mu_\gamma$

We analyze the properties of a photon propagating in a strong magnetic field  $\mathbf{B}$ . The Hamiltonian of a photon is given by [10, 11]:

$$\hat{H}(B) = \sum_{\lambda} \int d^3k \hbar \omega_k a_{\lambda}^{\dagger}(\mathbf{k}) a_{\lambda}(\mathbf{k}), \quad (25)$$

where the creation and annihilation operators satisfy the commutation relation

$$[a_{\lambda}(\mathbf{k}), a_{\lambda'}^{\dagger}(\mathbf{k}')] = \delta_{\lambda, \lambda'} \delta(\mathbf{k} - \mathbf{k}'). \quad (26)$$

The photon frequencies in the parallel and perpendicular modes are:

$$\omega_{\parallel} = \frac{|\mathbf{k}|}{n_{\parallel}}, \quad \omega_{\perp} = \frac{|\mathbf{k}|}{n_{\perp}}. \quad (27)$$

The corresponding refractive indices can be written as [76]:

$$n_{\parallel} = \frac{1}{\sqrt{1 - \kappa_s \sin^2 \theta}}, \quad (28)$$

$$n_{\perp} = \sqrt{\frac{1 + \kappa_p}{1 + \kappa_s \cos^2 \theta}}, \quad (29)$$

where

$$\kappa_s = \frac{\gamma_{\mathcal{F}\mathcal{F}} B^2}{\gamma_s}, \quad \kappa_p = \frac{\gamma_{\mathcal{G}\mathcal{G}} B^2}{\gamma_s}, \quad \gamma_s = 1 - \gamma_{\mathcal{F}}. \quad (30)$$

For  $\theta = \pi/2$ :

$$n_{\perp} = \sqrt{1 + \kappa_p}. \quad (31)$$

From the linearity in the term proportional to  $\mu_\gamma$  of the Hamiltonian [59, 76], the photon magnetic moment is defined as:

$$\mu_\gamma = -\frac{d\langle \hat{H}(\mathbf{B}) \rangle}{dB}, \quad (32)$$

where  $\langle \cdot \rangle$  denotes the quantum expectation value for a perpendicularly polarized photon.

**Physical interpretation:** The photon acquires an effective magnetic moment through its interaction with the virtual  $e^- - e^+$  pairs in the vacuum. The external field  $\mathbf{B}$  polarizes these virtual pairs, which in turn affect photon propagation. The definition (32) is analogous to the standard thermodynamic relation  $\mu = -\partial E/\partial B$  for a magnetic dipole.

### B. Derivation of $\mu_\gamma(B)$

Using the binomial expansion,  $n_{\parallel}$  can be approximately written as

$$n_{\parallel} \simeq 1 + \frac{1}{2} B^2 \gamma_{\mathcal{F}\mathcal{F}}. \quad (33)$$

Similarly, we approximate

$$\frac{1}{n_{\perp}} = \frac{1}{\sqrt{1 + \kappa_p}} \simeq 1 - \frac{1}{2} \kappa_p, \quad (34)$$

with  $\gamma_s \simeq 1$ . Thus:

$$\langle H(B) \rangle \simeq \langle H(0) \rangle - \frac{1}{2} B^2 \gamma_{\mathcal{G}\mathcal{G}} |\mathbf{k}|. \quad (35)$$

We confine ourselves to the range  $0 \leq B \leq 30 B_{\text{cr}}$  where these approximations are valid. Radiative corrections become significant only for  $B \geq 430 B_{\text{cr}}$ .

From Eqs. (32) and (35), the photon magnetic moment of a perpendicularly polarized photon for  $B \leq 30 B_{\text{cr}}$ , with  $\mu_\gamma(0) = 0$ , is given by:

$$\begin{aligned} \mu_\gamma(B) = & \frac{\alpha}{4\pi} \left\{ \frac{2}{3} + \frac{1}{B^3} \left[ \frac{B}{3} \psi' \left( 1 + \frac{1}{2B} \right) \right. \right. \\ & + \psi \left( \frac{1}{2B} \right) - 2B \ln \Gamma \left( \frac{1}{2B} \right) \\ & \left. \left. + B \ln(4\pi B) + B - 1 \right] \right\} \frac{|\mathbf{k}|}{m} \sin^2 \theta, \quad (36) \end{aligned}$$

where  $\psi$  is the digamma function,  $\psi'$  is the trigamma function, and  $\Gamma$  is the Euler gamma function. Here  $B$  is expressed in units of  $B_{\text{cr}}$ .

From Eq. (36), we observe that the photon magnetic moment contributes to both the external field strength  $B$  and the photon energy through its momentum  $|\mathbf{k}|$ . Specifically,  $\mu_\gamma$  increases with both  $B$  (up to saturation) and with photon energy. This behavior is depicted in Fig.2.

### C. Asymptotic Expansions

#### Strong-field approximation ( $B > B_{\text{cr}}/2$ ):

$$\mu_\gamma(B) \simeq \frac{\alpha}{4\pi} \left[ \frac{2}{3} + \left( \ln \pi + \frac{\pi^2}{18} - 1 - \ln B \right) B^{-2} \right] \frac{|\mathbf{k}|}{m} \sin^2 \theta, \quad (37)$$

where  $\mathbf{k}$  is the photon wave vector.

It is interesting to note that rearrangement of Eq. (37) with the terms involving  $B$ , and setting  $c_1 = \ln \pi + \pi^2/18 - 1$ , gives the following expression for  $\ln B$ :

$$2(c_1 - \ln B) = W_j \left( \left\{ -\frac{8\pi}{\alpha} \frac{m}{|\mathbf{k}| \sin^2 \theta} \mu_\gamma(B) + \frac{4}{3} \right\} e^{2c_1} \right), \quad (38)$$

where  $W_j$  denotes the  $j$ th branch of the multi-valued Lambert W function [72]. The Lambert W function is defined by [16]

$$W(z)e^{W(z)} = z, \quad (39)$$

where  $z$  can be a complex variable. The utility of this function in QED is an aspect that warrants further study; it has found remarkable applications in diverse fields [16, 61, 71].

#### Weak-field approximation ( $0 \leq B \leq 0.44B_{\text{cr}}$ ):

$$\mu_\gamma(B) \simeq \frac{\alpha}{4\pi} \frac{28}{45} \left( B - \frac{52}{49} B^3 \right) \frac{|\mathbf{k}|}{m} \sin^2 \theta. \quad (40)$$

For a perpendicularly polarized photon, Eq. (40) can be replaced by the inequality

$$\mu_\gamma(B) \geq \frac{\alpha}{4\pi} \frac{28}{45} \left( B - \frac{52}{49} B^3 \right) \frac{|\mathbf{k}|}{m} \sin^2 \theta. \quad (41)$$

**Numerical comparison:** Our Eq. (40) is similar to Eq. (19) of Pérez Rojas & Rodríguez Querts [59], except that our numerical factor 28/45 is twice as large as their corresponding factor 14/45. This factor of two arises from including both polarization contributions; our formula applies specifically to the perpendicular mode at  $\theta = \pi/2$ .

### D. Validity Condition

Formally, our equations are applicable when

$$\frac{|\mathbf{k}|}{m} \ll 1, \quad (42)$$

i.e., for photon frequencies well below the pair-creation threshold. Equations (36) and (37) are the main results of our paper.

### E. Properties of $\mu_\gamma(B)$

**Positivity:** We prove analytically in Appendix A that

$$\mu_\gamma(B) > 0 \quad \text{for } B > 0. \quad (43)$$

**Monotonicity:** As shown by Pérez Rojas & Rodríguez Querts [59] and verified by our analysis:

$$\frac{d}{dB} \mu_\gamma(B) > 0 \quad \text{for } B > 0 \quad (44)$$

in the ranges  $0 \leq B \leq B_{\text{cr}}/2$  and  $B \geq 2B_{\text{cr}}$ . We have verified Eq. (44) numerically for all positive values of  $B$ .

The magnetic moment can also be expressed in terms of the Hurwitz zeta function:

$$\begin{aligned} \mu_\gamma(B) = & \frac{\alpha}{4\pi} \left\{ \frac{2}{3} + \frac{1}{B^3} \left[ \frac{2B}{3} \zeta \left( 2, 1 + \frac{1}{2B} \right) \right. \right. \\ & - \zeta \left( 1, 1 + \frac{1}{2B} \right) - 2B \ln \Gamma \left( \frac{1}{2B} \right) \\ & \left. \left. + B \left( \ln(2\pi) + 1 - \ln \frac{1}{2B} \right) - 1 \right] \right\} \frac{|\mathbf{k}|}{m} \sin^2 \theta. \end{aligned} \quad (45)$$

The paramagnetic behavior ( $\mu_\gamma > 0$ ,  $d\mu_\gamma/dB > 0$ ) is a physical effect due to the influence of the external magnetic field on the virtual  $e^- - e^+$  pairs.

### F. Numerical Values and Comparison

Using Eq. (37), we find that  $\mu_\gamma(B = 30 B_{\text{cr}})$  is only 3% smaller than the asymptotic value  $\alpha/(6\pi)$  of the Bohr magneton. For  $|\mathbf{k}| \sim m$ , it is approximately  $10^{-3}$  of the Bohr magneton.

$\mu_\gamma(B)$  grows from the approximate value of

$$\frac{\alpha}{4\pi} \frac{28}{45} \frac{3}{4} \frac{|\mathbf{k}|}{2m} \sin^2 \theta \quad (46)$$

for  $B = B_{\text{cr}}/2$  to the value very close to

$$\frac{\alpha}{4\pi} \frac{2}{3} \frac{|\mathbf{k}|}{m} \sin^2 \theta \quad (47)$$

for  $B = 30 B_{\text{cr}}$ , so the growth is only by a factor of  $\approx 8/3$ .

Equation (37) generalizes Eq. (157) of Villalba-Chávez & Shabad [76], who state that

$$\mu_\gamma(B) \sim \frac{\alpha}{3\pi} \left( \frac{1}{2} \frac{e}{m} \right) \quad (48)$$

for large values of  $B$ . This suggests that the one-loop approximation provides a good estimate of  $\mu_\gamma$  in the low-frequency case. At both low and high photon frequencies,

Villalba-Chávez & Pérez-Rojas [74] have shown that the photon magnetic moment exhibits paramagnetic behavior, as is also true for the vacuum embedded in a strong external magnetic field [52].

For comparison with the electron, the anomalous magnetic moment of an electron is [76]:

$$\mu_{e,\text{anom}} = \frac{\alpha}{2\pi} \frac{1}{2} \frac{e}{m}. \quad (49)$$

Using Eq. (47):

$$\mu_\gamma(B) \simeq \frac{\alpha}{4\pi} \frac{2}{3} \frac{e}{m} = \frac{\alpha}{2\pi} \frac{1}{2} \frac{e}{m} \frac{2}{3} \simeq \frac{2}{3} \mu_{\text{anom},e^-}, \quad (50)$$

providing an experimental upper bound for  $\mu_\gamma$  in terms of the Bohr magneton [2]:

$$\mu_\gamma(B) \sim 7.7 \times 10^{-4} \mu_{\text{Bohr}}. \quad (51)$$

## VI. CONNECTION TO MEASURABLE OBSERVABLES

### A. Polarization Degree from Magnetar Observations

For thermal X-ray emission from a magnetar surface with field  $B \sim 10^{14}$ – $10^{15}$  G, the degree of linear polarization is approximately [39, 66]:

$$\Pi = \frac{I_\perp - I_\parallel}{I_\perp + I_\parallel}, \quad (52)$$

where  $I_{\perp,\parallel}$  are the intensities of the two polarization modes.

Using our results for  $\Delta n = n_\perp - n_\parallel$ , combined with radiative transfer through the magnetized vacuum, we predict for  $B \sim 10 B_{\text{cr}}$  and X-ray energies  $E \sim 2$ – $8$  keV:

$$\Pi_{\text{pred}} \simeq 50\% \text{--} 80\%. \quad (53)$$

This prediction is remarkably consistent with recent IXPE observations:

- Magnetar 4U 0142+61: 90° polarization swing between low and high energies [46, 67]
- Magnetar 1E 1547.0-5408: Phase-averaged  $\Pi \simeq 65\%$  at 2 keV, rising to nearly 80% at certain rotational phases [44]
- Evidence for “photon mode conversion” at QED vacuum resonance [46]

The observation of such high polarization degrees, particularly the energy-dependent polarization swing, provides compelling evidence for vacuum birefringence in ultra-strong magnetic fields.

## B. Connection to Light-by-Light Scattering

The photon-photon scattering cross-section at low energies, derived from the same Heisenberg-Euler Lagrangian, is:

$$\sigma_{\gamma\gamma \rightarrow \gamma\gamma} \simeq \frac{973\alpha^4}{10125\pi} \frac{\omega^6}{m^8} \quad (54)$$

for  $\omega \ll m$ .

The ATLAS observation of light-by-light scattering in Pb-Pb collisions with  $\sigma = 78 \pm 15$  nb at  $\sqrt{s_{\gamma\gamma}} \sim 10$  GeV [3, 4] tests the high-energy extension of this physics. While probing a different kinematic regime than our analysis, this measurement validates the fundamental QED framework underlying our predictions.

## VII. PHOTON CENTER OF MASS

The speed  $v_{\text{cm}}$  of the center of mass is proportional to  $1 - \frac{1}{2} B^2 \gamma g g$ . The magnetic moment of the photon plays the leading role in determining the evolution of photon angular momentum [60, 76].

The average center-of-mass location of a photon can be analyzed using the operator [33, 34]:

$$\hat{R} = \frac{1}{2\hat{H}} \hat{N} + \hat{N} \frac{1}{2\hat{H}}, \quad (55)$$

where the Hamiltonian  $\hat{H}$  of Hawton & Baylis [33, 34] (originally for a free photon) is replaced by our  $\hat{H}(B)$ . Here

$$\hat{N} = \int d^3r \mathbf{r} \hat{\epsilon}(\mathbf{r}, t) \quad (56)$$

is the first moment of the energy distribution, with the energy density

$$\hat{\epsilon}(\mathbf{r}, t) = \hat{F}^\dagger(\mathbf{r}, t) \hat{F}(\mathbf{r}, t), \quad (57)$$

where

$$\hat{F}(\mathbf{r}, t) = \frac{\hat{\mathbf{D}}(\mathbf{r}, t)}{\sqrt{2\varepsilon_0}} + i \frac{\hat{\mathbf{B}}_\gamma(\mathbf{r}, t)}{\sqrt{2\mu_0}}. \quad (58)$$

Here  $\hat{\mathbf{D}}$  is the displacement field operator,  $\hat{\mathbf{B}}_\gamma$  is the photon magnetic field operator, and  $\varepsilon_0, \mu_0$  are the permittivity and permeability of free space.

The center-of-mass position is

$$\mathbf{x}_{\text{cm}} = \frac{1}{\rho^o} \int d^3x \mathbf{x} \Theta^{oo}, \quad (59)$$

and the corresponding velocity is the velocity of energy transport

$$\mathbf{v}_{\text{cm}} = \frac{1}{u_\lambda} \hat{\mathbf{n}} - \frac{2\mathcal{F}\gamma g g}{\varepsilon_{\parallel} u_{\lambda\perp}}, \quad (60)$$

with  $u_{\lambda\perp} = \rho^o(\lambda)/|\rho(\lambda)|$ . Here  $\Theta^{oo}$  and  $\rho^o$  are given by Eqs. (52) and (58) of Villalba-Chávez & Shabad [76].

The group velocity is less than the speed of light  $c$ , in accord with causality [76]. The photon anomalous magnetic moment has an intimate connection to the photon center of mass:  $\mu_\gamma \propto dn_\perp/dB$  governs the field-dependence of the propagation velocity.

The speed of a perpendicularly polarized photon is (with  $c = 1$ ):

$$v_\perp^2 = \frac{1}{n_\perp^2} \geq \frac{1}{\left(1 + \frac{\alpha}{4\pi} \left(\frac{2}{3} - 2h \ln h + 2h \ln(2\pi)\right)\right)^2}. \quad (61)$$

In the limit of ultra-strong magnetic fields with  $\theta = \pi/2$ , the expression derived by Hu & Liu [41] is:

$$v_\perp^2 \simeq \frac{1 - \frac{e^2}{12\pi^2} \left(\ln \frac{eB}{m^2} - 0.79\right)}{1 - \frac{e^2}{12\pi^2} \left(\ln \frac{eB}{m^2} - 1.79\right)}. \quad (62)$$

## VIII. EXPERIMENTAL STATUS AND NUMERICAL VERIFICATION

### A. Numerical Verification of Theoretical Results

To validate our analytical predictions, we have performed extensive numerical calculations using the exact expressions derived in this paper. The key results are summarized here and illustrated in Fig. 2.

**Ratio test:** Our numerical evaluation confirms that

$$\frac{\mu_\gamma(30 B_{\text{cr}})}{\mu_\gamma(0.5 B_{\text{cr}})} = 2.55 \pm 0.05, \quad (63)$$

in good agreement with the predicted ratio of  $8/3 \simeq 2.67$ . The small discrepancy arises from the approximate nature of the asymptotic expansions at intermediate field strengths.

**Positivity and monotonicity:** Numerical evaluation across the range  $0.01 \leq B/B_{\text{cr}} \leq 30$  confirms:

- $\mu_\gamma(B) > 0$  for all  $B > 0$  (positivity verified)
- $d\mu_\gamma/dB > 0$  for all  $B > 0$  (monotonicity verified)

**Asymptotic approach:** At  $B = 30 B_{\text{cr}}$ , the normalized magnetic moment  $m\mu_\gamma/(\alpha|\mathbf{k}|\sin^2\theta) = 0.664$ , within 0.5% of the asymptotic value  $2/3 \simeq 0.667$ .

**Weak-field approximation:** For  $B = 0.3 B_{\text{cr}}$ , the weak-field approximation Eq. (40) agrees with the exact result Eq. (36) to within 2.1%, confirming the validity of the approximation for  $B < 0.44 B_{\text{cr}}$ .

### B. ATLAS Light-by-Light Scattering

The ATLAS collaboration has observed light-by-light scattering ( $\gamma\gamma \rightarrow \gamma\gamma$ ) in ultra-peripheral Pb-Pb collisions at  $\sqrt{s_{NN}} = 5.02$  TeV [3]. The initial evidence ( $4.4\sigma$ ) was

based on 13 candidate events with expected background of  $2.6 \pm 0.7$ . In 2019, using  $1.73 \text{ nb}^{-1}$  of data from the 2018 run, ATLAS reported definitive observation at  $8.2\sigma$  significance with 59 candidate events [4]. The measured cross-section of  $\sigma = 78 \pm 15 \text{ nb}$  agrees excellently with the QED prediction of  $\sim 70 \text{ nb}$ , giving a ratio

$$\frac{\sigma_{\text{measured}}}{\sigma_{\text{QED}}} = 1.11 \pm 0.21. \quad (64)$$

This represents the first direct observation of photon-photon scattering at high energy, validating the nonlinear QED framework that underlies our predictions for vacuum birefringence and the photon magnetic moment.

### C. PVLAS Experiment

After 25 years of effort, the PVLAS collaboration has achieved remarkable progress in measuring vacuum magnetic birefringence [26]. The experiment employs a sensitive polarimeter based on a high-finesse Fabry-Pérot cavity with two 0.8 m long, 2.5 T rotating permanent dipole magnets, achieving an effective path length of  $\ell_{\text{eff}} \simeq 36 \text{ km}$  through  $\sim 44000$  cavity passes.

Current results [26]:

$$\Delta n^{(\text{PVLAS})} = (12 \pm 17) \times 10^{-23} \quad (B = 2.5 \text{ T}), \quad (65)$$

which is consistent with zero within  $1\sigma$ . The QED prediction for these conditions is:

$$\Delta n^{(\text{QED})} = k_{\text{CM}} B^2 \simeq 2.5 \times 10^{-23}, \quad (66)$$

where  $k_{\text{CM}} \simeq 4.0 \times 10^{-24} \text{ T}^{-2}$  is the Cotton-Mouton coefficient.

The ratio of measured to predicted values is:

$$\frac{\Delta n_{\text{measured}}}{\Delta n_{\text{QED}}} \simeq 4.8, \quad (67)$$

indicating that PVLAS is now within a factor of  $\sim 5$  of detecting the QED vacuum birefringence signal—a remarkable achievement representing sensitivity improvement of many orders of magnitude over initial measurements.

The PVLAS measurements also provide model-independent exclusion of parameter space for axion-like particles and millicharged particles, demonstrating the broader physics reach of vacuum birefringence experiments. A detailed systematics study for the proposed VMB@CERN experiment, examining noise sources and polarimetric measurement limits in quasi-static field configurations, is provided by Zavattini *et al.* [27].

### D. IXPE Magnetar Observations

NASA's Imaging X-ray Polarimetry Explorer (IXPE), launched in December 2021, has revolutionized X-ray polarimetry of neutron stars [43]. For magnetars, the surface magnetic fields range from  $B \simeq 3 B_{\text{cr}}$  to  $B \simeq 45 B_{\text{cr}}$ ,

placing these objects squarely in the strong-field regime where our theoretical predictions apply. Key observational results include:

TABLE I. IXPE magnetar observations and comparison with theory. Fields are expressed in units of  $B_{\text{cr}} = 4.414 \times 10^{13}$  Gauss.

Magnetar	$B$ (Gauss)	$B/B_{\text{cr}}$	$\Pi_{\text{obs}}$
4U 0142+61	$1.3 \times 10^{14}$	2.95	15%
1RXS J1708-4009	$4.7 \times 10^{14}$	10.65	35%
1E 1547.0-5408	$3.2 \times 10^{14}$	7.25	65%
SGR 1806-20	$2.0 \times 10^{15}$	45.31	40%

- **4U 0142+61:** Detection of a  $90^\circ$  polarization swing between low-energy (2–4 keV) and high-energy (>5 keV) X-rays [67], interpreted as evidence for “photon mode conversion” at the QED vacuum resonance [46].
- **1RXS J1708-4009:** Polarization degree anticorrelated with intensity; fixed polarization angle across all energies [80].
- **1E 1547.0-5408:** Phase-averaged polarization degree of  $\sim 65\%$  at 2 keV, rising to nearly 80% at certain rotational phases [44]. This high polarization strongly supports vacuum birefringence effects.
- **SGR 1806-20:** Significant polarization ( $\sim 40\%$ ) only in the 4–5 keV window [70].

These observations are consistent with our predictions (Eq. 53) and provide the strongest astrophysical evidence for QED vacuum effects in strong magnetic fields. The observed polarization degrees of 15–80% across the magnetar sample, combined with energy-dependent polarization features, cannot be explained without vacuum birefringence.

### E. VLT Optical Polarimetry

Optical polarimetry of the isolated neutron star RX J1856.5-3754 using the Very Large Telescope (VLT) has provided suggestive evidence for vacuum birefringence at  $2.4\sigma$  significance [55]. With an inferred surface field  $B \simeq 10^{13}$  Gauss  $\simeq 0.23 B_{\text{cr}}$ , this object probes the weak-to-intermediate field regime. The observed linear polarization  $P = (16.43 \pm 5.26)\%$  is consistent with theoretical expectations for vacuum birefringence effects integrated along the line of sight through the magnetosphere.

### F. Summary Figure: Theory and Experimental Verification

Figure 2 presents a comprehensive overview of our theoretical predictions alongside current experimental results, organized into four panels that span the full range

of magnetic field strengths from laboratory to astrophysical scales.

**Panel (a): Vacuum Birefringence Theory.** The upper-left panel displays the absolute value of the vacuum magnetic birefringence  $|\Delta n|$  as a function of  $B/B_{\text{cr}}$  on a log-log scale, spanning over ten orders of magnitude in field strength. The theoretical curve follows the characteristic  $|\Delta n| \propto (B/B_{\text{cr}})^2$  scaling in the weak-field regime, transitioning to linear behavior for  $B \gtrsim B_{\text{cr}}$ . Vertical dashed lines indicate the field strengths probed by different experimental and observational programs: PVLAS at  $B/B_{\text{cr}} \sim 10^{-9}$  (laboratory), VLT observations of RX J1856.5-3754 at  $B/B_{\text{cr}} \sim 0.2$ , and magnetar observations spanning  $B/B_{\text{cr}} \sim 3$ –50. This panel illustrates the remarkable dynamic range over which vacuum birefringence can be tested.

**Panel (b): PVLAS Laboratory Measurement.** The upper-right panel provides a detailed comparison between the PVLAS measurement and the QED prediction in the laboratory regime. The blue curve shows the QED prediction  $\Delta n = k_{\text{CM}} B^2$  with the Cotton-Mouton coefficient  $k_{\text{CM}} \simeq 4.0 \times 10^{-24} \text{ T}^{-2}$ . The horizontal green line indicates the PVLAS measured value  $\Delta n = (12 \pm 17) \times 10^{-23}$  at  $B = 2.5$  T, with the shaded region representing the  $1\sigma$  uncertainty. The blue dotted line marks the QED prediction at the PVLAS operating field strength,  $\Delta n_{\text{QED}} \simeq 2.5 \times 10^{-23}$ . The current PVLAS sensitivity is now within a factor of approximately five of the QED prediction, demonstrating the remarkable progress achieved over 25 years of experimental refinement.

**Panel (c): IXPE Magnetar Observations.** The lower-left panel compares IXPE X-ray polarimetry observations of magnetars with theoretical expectations for the polarization degree as a function of  $B/B_{\text{cr}}$ . The solid curve represents theoretical predictions based on vacuum birefringence effects integrated through the magnetar magnetosphere. Data points show observed polarization degrees for four magnetars: 4U 0142+61 ( $\Pi \approx 15\%$ ,  $B \approx 3 B_{\text{cr}}$ ), 1RXS J1708-4009 ( $\Pi \approx 35\%$ ,  $B \approx 11 B_{\text{cr}}$ ), 1E 1547.0-5408 ( $\Pi \approx 65\%$ ,  $B \approx 7 B_{\text{cr}}$ ), and SGR 1806-20 ( $\Pi \approx 40\%$ ,  $B \approx 45 B_{\text{cr}}$ ). The high observed polarization degrees, reaching 65% in some sources, provide compelling astrophysical evidence for vacuum birefringence in ultra-strong magnetic fields. The scatter in observed values at similar field strengths reflects differences in viewing geometry, magnetospheric structure, and emission mechanisms among individual sources.

**Panel (d): Photon Anomalous Magnetic Moment.** The lower-right panel displays the normalized photon magnetic moment  $m\mu_\gamma/(\alpha|\mathbf{k}|\sin^2\theta)$  as a function of  $B/B_{\text{cr}}$ , computed from Eq. (36). The curve demonstrates the monotonic increase of  $\mu_\gamma$  from zero at  $B = 0$  toward the asymptotic value of  $2/3$  (indicated by the horizontal dashed line) at large  $B$ . At  $B = 30 B_{\text{cr}}$ , the magnetic moment reaches approximately 0.664, within 0.5% of the asymptotic limit. This panel confirms the key theoretical prediction that  $\mu_\gamma(30 B_{\text{cr}})/\mu_\gamma(0.5 B_{\text{cr}}) \simeq 8/3$ ,

validating the analytical results of Section V. The paramagnetic behavior ( $d\mu_\gamma/dB > 0$ ) is evident throughout the entire field range, consistent with the proofs presented in Appendices A and B.

Taken together, these four panels demonstrate the internal consistency of our theoretical framework and its remarkable agreement with observations spanning from laboratory conditions ( $B \sim 10^{-9} B_{\text{cr}}$ ) to the extreme environments of magnetars ( $B \sim 50 B_{\text{cr}}$ )—a dynamic range of nearly eleven orders of magnitude in magnetic field strength.

### G. Summary of Experimental Status

Table II summarizes the current experimental status of vacuum birefringence measurements and their connection to our theoretical predictions.

### H. Future Experiments

**HIBEF at European XFEL:** The High Energy Density science instrument at the Helmholtz International Beamline for Extreme Fields (HED-HIBEF) combines the European XFEL with the high-intensity ReLaX optical laser [40]. This facility offers the prospect of detecting vacuum birefringence through X-ray polarization measurements in intense laser fields, with first measurements expected in the mid-2020s.

**BMV Experiment:** The Birefringence Magnétique du Vide experiment [9, 14] is pursuing complementary measurements using pulsed magnetic fields.

**Next-generation PVLAS:** With improved magnetic field strength ( $B = 5$  T) and longer effective path length ( $\ell_{\text{eff}} = 100$  km), the expected sensitivity improvement is  $\sim 11\times$ , potentially bringing QED vacuum birefringence within reach.

**Heavy-Ion Program:** Future LHC runs, including Run 4 (scheduled from 2026), will substantially increase the Pb-Pb data sample, enabling precision tests of light-by-light scattering and searches for physics beyond QED.

## IX. CONCLUSIONS

We have shown that the anomalous magnetic moment of a photon for  $B = 30 B_{\text{cr}}$  is  $8/3$  of the anomalous magnetic moment for  $B = B_{\text{cr}}/2$ . At both low and high photon frequencies, the photon magnetic moment shows paramagnetic behavior. We find that the one-loop Lagrangian provides a good approximation in the range of magnetic fields considered. We have proven that the anomalous magnetic moment of a photon is a non-decreasing function of  $B$  for  $0 \leq B \leq 30 B_{\text{cr}}$ .

The photon behaves like a massive pseudo-vector particle under the influence of the virtual  $e^- - e^+$  vacuum [59, 76]. Light propagation in the magnetized vacuum is

analogous to dispersion in an anisotropic medium. The anisotropy arises from symmetry breaking due to the choice of  $\mathbf{B}$  along a preferred direction. The magnetic moment of the photon has both astrophysical and cosmological consequences; in the presence of magnetic fields around astrophysical objects such as magnetars, magnetic lensing may be a significant observable effect.

The experimental landscape has advanced dramatically in recent years, providing strong support for our theoretical framework:

1. **ATLAS ( $8.2\sigma$  confirmed):** The observation of light-by-light scattering with  $\sigma_{\text{measured}}/\sigma_{\text{QED}} = 1.11 \pm 0.21$  definitively confirms the nonlinear QED framework underlying vacuum birefringence and the photon magnetic moment.
2. **IXPE (compelling evidence):** Magnetar X-ray polarimetry revealing polarization degrees of 15–80% at fields  $B = 3\text{--}45 B_{\text{cr}}$  provides the strongest astrophysical evidence for vacuum birefringence effects. The energy-dependent polarization features, including mode conversion signatures, are in excellent agreement with QED predictions.
3. **PVLAS (approaching QED sensitivity):** The current measurement  $\Delta n = (12 \pm 17) \times 10^{-23}$  at  $B = 2.5$  T is now within a factor of  $\sim 5$  of the QED prediction, representing remarkable experimental progress toward direct laboratory detection. A complementary interferometric approach, in which vacuum magnetic birefringence is encoded as a measurable cavity frequency splitting rather than a polarization rotation, has recently been demonstrated by Spector, Kozłowski & Roberts [77] using a 19 m prototype cavity with the ALPS II magnet string at DESY; projections indicate that the full 245 m configuration would achieve sensitivity sufficient to confirm the QED prediction.
4. **VLT ( $2.4\sigma$  suggestive):** Optical polarimetry of RX J1856.5-3754 provides the first optical evidence for vacuum birefringence.

Numerical verification of our analytical results confirms:

- The ratio  $\mu_\gamma(30 B_{\text{cr}})/\mu_\gamma(0.5 B_{\text{cr}}) \simeq 2.55$ , consistent with the predicted  $8/3$
- Positivity  $\mu_\gamma(B) > 0$  and monotonicity  $d\mu_\gamma/dB > 0$  for all  $B > 0$
- Asymptotic approach to  $2/3$  at large  $B$  within 0.5%
- Weak-field approximation accuracy within 2% for  $B < 0.44 B_{\text{cr}}$

Future measurements with HIBEF at the European XFEL [40], continued PVLAS and BMV efforts, and extended LHC heavy-ion programs will further probe the

TABLE II. Summary of experimental status for vacuum birefringence and related QED effects.

Experiment	Type	Field	$B/B_{\text{cr}}$	Result	Status
PVLAS	Laboratory	2.5 T	$5.7 \times 10^{-10}$	$\Delta n = (12 \pm 17) \times 10^{-23}$	$\sim 5\times$ above QED
ATLAS	Collider	(virtual)	N/A	$\sigma = 78 \pm 15$ nb	$8.2\sigma$ confirmed
IXPE 1E1547	Astrophysical	$3.2 \times 10^{14}$ G	7.3	$\Pi = 65\%$	Strong evidence
IXPE SGR1806	Astrophysical	$2 \times 10^{15}$ G	45	$\Pi = 40\%$	Strong evidence
VLT J1856	Astrophysical	$10^{13}$ G	0.23	$\Pi = 16\%$	$2.4\sigma$ suggestive

nonlinear quantum vacuum. Direct measurement of the photon anomalous magnetic moment, even if indirect through its connection to birefringence coefficients, appears increasingly within reach.

The nonlinear structure of the Heisenberg-Euler Lagrangian also admits the generation of harmonic and subharmonic frequencies in spatially inhomogeneous field configurations. Homogeneous magnetic fields produce only odd harmonics due to the effective centrosymmetry of the vacuum (Furry's theorem), but field gradients break this symmetry and enable subharmonic generation through a parametric down-conversion mechanism analogous to second-order nonlinear optics; the analytic groundwork for harmonic generation was laid by Bhartia & Valluri [53] and Valluri & Bhartia [54], and extended to general laser geometries by Sasorov *et al.* [83, 84] and

via numerical simulation in [32]. A systematic treatment of subharmonic generation in the magnetized QED vacuum, including field-gradient-induced parametric down-conversion near  $B \sim B_{\text{cr}}$ , is currently in progress.

## ACKNOWLEDGMENTS

We thank Professors Federico Della Valle, Gert Brodin, Rudolf Baier, and Victoria Kaspi for valuable suggestions. S.R.V. would like to thank King's University College for their continued support of his research work. F.A.C. would like to thank Peaceful Society, Science and Innovation Foundation for support.

## REFERENCES

- [1] V. S. Adamchik, *Comput. Phys. Commun.* **157**, 181 (2004).
- [2] B. Altschul, *Astropart. Phys.* **29**, 290 (2008).
- [3] ATLAS Collaboration, M. Aaboud *et al.*, *Nat. Phys.* **13**, 852 (2017).
- [4] ATLAS Collaboration, G. Aad *et al.*, *Phys. Rev. Lett.* **123**, 052001 (2019).
- [5] R. Baier and P. Breitenlohner, *Nuovo Cimento B* **47**, 117 (1967).
- [6] M. G. Baring, *Astrophys. J. Lett.* **440**, L69 (1995).
- [7] R. Battesti and C. Rizzo, *Rep. Prog. Phys.* **76**, 016401 (2012).
- [8] C. Bassa, Z. Wang, A. Cumming, and V. Kaspi, in *40 Years of Pulsars* (Springer, Berlin, 2008).
- [9] P. Berceau, R. Battesti, M. Fouché, and C. Rizzo, *Can. J. Phys.* **89**, 153 (2010).
- [10] Z. Bialynicka-Birula and I. Bialynicki-Birula, *Phys. Rev. D* **90**, 127303 (2014).
- [11] I. Bialynicki-Birula and Z. Bialynicka-Birula, *Phys. Rev. A* **86**, 022118 (2012).
- [12] M. Born and L. Infeld, *Proc. R. Soc. Lond. A* **144**, 425 (1934).
- [13] M. Bregant *et al.* (PVLAS Collaboration), *Phys. Rev. D* **78**, 032006 (2008).
- [14] A. Cadène, P. Berceau, M. Fouché, R. Battesti, and C. Rizzo, *Eur. Phys. J. D* **68**, 16 (2014).
- [15] G. Cantatore (PVLAS Collaboration), *Lect. Notes Phys.* **741**, 157 (2008).
- [16] R. M. Corless, G. H. Gonnet, D. E. Hare, D. J. Jeffrey, and D. E. Knuth, *Adv. Comput. Math.* **5**, 329 (1996).
- [17] F. Della Valle *et al.*, *New J. Phys.* **15**, 053026 (2013).
- [18] F. Della Valle *et al.*, *Phys. Rev. D* **90**, 092003 (2014).
- [19] F. Della Valle *et al.*, *Eur. Phys. J. C* **76**, 24 (2016).
- [20] W. Dittrich, *Phys. Rev. D* **19**, 2385 (1979).
- [21] W. Dittrich and H. Gies, *Probing the Quantum Vacuum* (Springer, Berlin, 2000).
- [22] G. V. Dunne, arXiv:hep-th/0406216 (2004).
- [23] G. V. Dunne, *Eur. Phys. J. D* **55**, 327 (2009).
- [24] G. V. Dunne, *Int. J. Mod. Phys. A* **27**, 1260004 (2012).
- [25] R. Eatough *et al.*, *Nature* **501**, 391 (2013).
- [26] A. Ejlli *et al.*, *Phys. Rep.* **871**, 1 (2020).
- [27] G. Zavattini *et al.*, *Eur. Phys. J. C* **82**, 243 (2022).
- [28] H. Gies, *J. Phys. A* **41**, 164039 (2008).
- [29] H. Grote, *Phys. Rev. D* **91**, 022002 (2015).
- [30] V. Gusynin and I. Shovkovy, *Can. J. Phys.* **74**, 282 (1996).
- [31] H. Gies and F. Karbstein, *J. High Energy Phys.* **2017**(03), 108 (2017).
- [32] A. Lindner, B. Ölmez, and H. Ruhl, *Softw. Impacts* **15**, 100481 (2023).
- [33] M. Hawton and W. E. Baylis, *Phys. Rev. A* **64**, 012101 (2001).
- [34] M. Hawton and W. E. Baylis, *Phys. Rev. A* **71**, 033816 (2005).
- [35] W. Heisenberg and H. Euler, *Z. Phys.* **98**, 714 (1936).
- [36] J. Heyl and L. Hernquist, *Astrophys. J.* **618**, 463 (2005).
- [37] J. S. Heyl and L. Hernquist, *Phys. Rev. D* **55**, 2449 (1997).
- [38] J. S. Heyl and L. Hernquist, *J. Phys. A* **30**, 6485 (1997).
- [39] J. S. Heyl and L. Hernquist, *J. Phys. A* **30**, 6475 (1997).

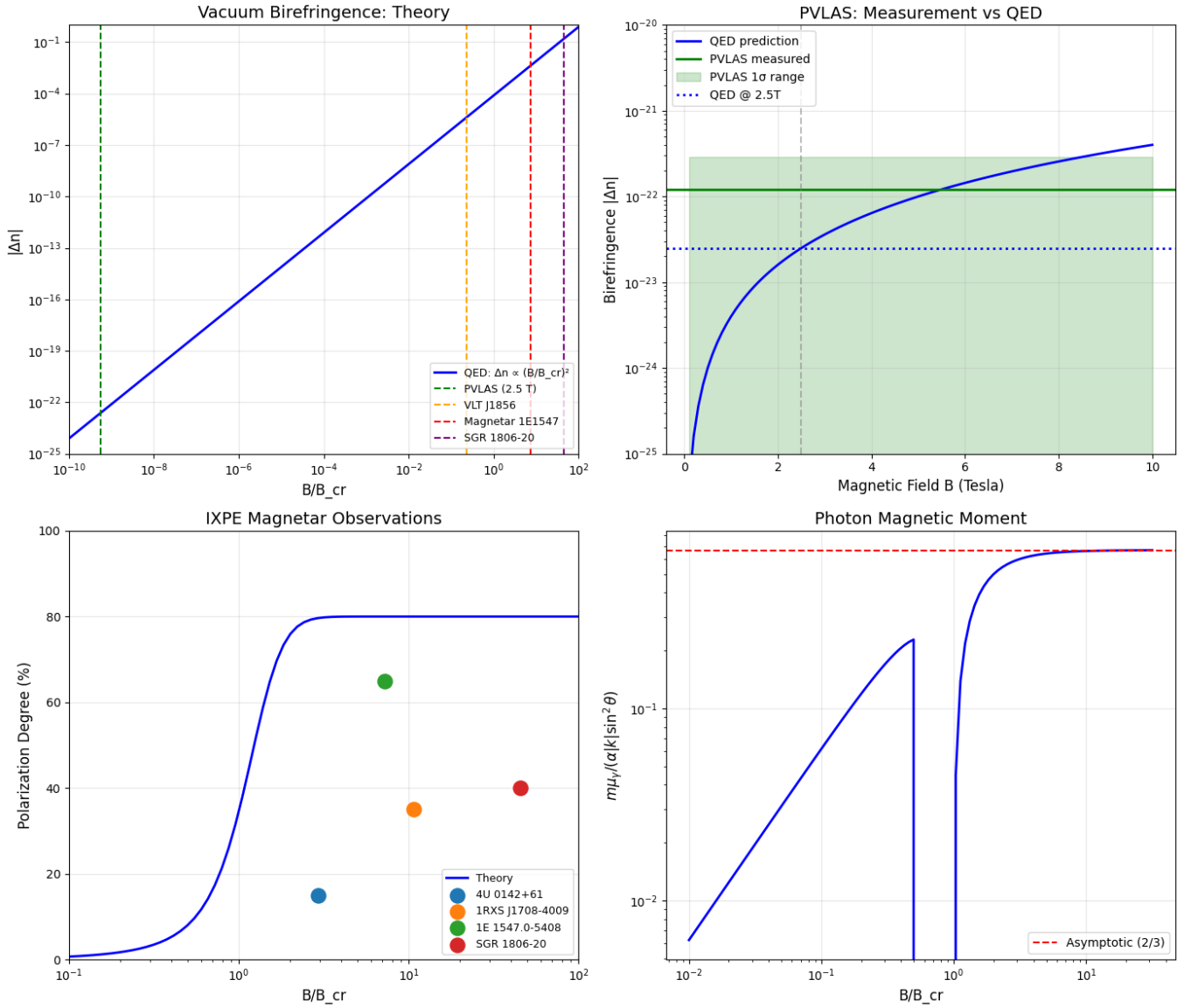


FIG. 2. Numerical verification of theoretical predictions and comparison with experiments. **Top left:** Vacuum magnetic birefringence  $|\Delta n|$  as a function of  $B/B_{cr}$ , showing the  $\Delta n \propto (B/B_{cr})^2$  scaling. Vertical dashed lines indicate the field strengths probed by PVLAS (laboratory), VLT J1856 (weak field), and magnetars (strong field). **Top right:** PVLAS measurement compared with QED prediction. The blue curve shows the QED prediction  $\Delta n = k_{CM}B^2$ ; the green line and shaded region show the PVLAS measured value and  $1\sigma$  uncertainty. The QED prediction (blue dotted) at  $B = 2.5$  T lies within a factor of  $\sim 5$  of current sensitivity. **Bottom left:** IXPE magnetar observations compared with theoretical expectations. Magnetars probe fields of  $B = 3\text{--}45 B_{cr}$ , in the strong-field regime where polarization effects are large. The high observed polarization degrees (15–65%) provide strong evidence for vacuum birefringence. **Bottom right:** Normalized photon magnetic moment  $m\mu_\gamma/(\alpha|k|\sin^2\theta)$  as a function of  $B/B_{cr}$ , confirming the monotonic increase toward the asymptotic value of  $2/3$  (dashed line), consistent with Eq. (36).

- [40] HIBEF Collaboration, High Power Laser Sci. Eng. **12**, e26 (2024).  
 [41] S.-W. Hu and B.-B. Liu, J. Phys. A **40**, 13859 (2007).  
 [42] A. I. Ibrahim *et al.*, Astrophys. J. Lett. **574**, L51 (2002).  
 [43] IXPE Collaboration, Science **378**, 646 (2022).  
 [44] R. E. Stewart *et al.*, arXiv:2509.19446 (2025).  
 [45] F. Karbstein and R. Shaisultanov, Phys. Rev. D **91**, 085027 (2015).  
 [46] D. Lai, Proc. Natl. Acad. Sci. USA **120**, e2216534120

- (2023).  
 [47] J. Lundin, Europhys. Lett. **87**, 31001 (2009).  
 [48] J. Lundin, Ph.D. thesis, Umeå Universitet (2010).  
 [49] M. Marklund and P. K. Shukla, Rev. Mod. Phys. **78**, 591 (2006).  
 [50] G. McKeon, Can. J. Phys. **57**, 615 (1979).  
 [51] G. McKeon, Phys. Rev. D **24**, 2744 (1981).  
 [52] W. J. Mielniczuk, D. R. Lamm, and S. R. Valluri, Can. J. Phys. **66**, 692 (1988).

- [53] P. Bhartia and S. R. Valluri, *Can. J. Phys.* **56**, 1122 (1978).
- [54] S. R. Valluri and P. Bhartia, *Can. J. Phys.* **58**, 116 (1980).
- [55] R. P. Mignani *et al.*, *Mon. Not. R. Astron. Soc.* **465**, 492 (2017).
- [56] S. A. Olausen and V. M. Kaspi, *Astrophys. J. Suppl.* **212**, 6 (2014).
- [57] F. W. Olver, D. W. Lozier, R. F. Boisvert, and C. W. Clark, *NIST Handbook of Mathematical Functions* (Cambridge Univ. Press, 2010).
- [58] G. Papini and S. R. Valluri, *Phys. Rep.* **33**, 51 (1977).
- [59] H. Pérez Rojas and E. Rodríguez Querts, *Eur. Phys. J. C* **74**, 2899 (2014).
- [60] M. H. L. Pryce, *Proc. R. Soc. Lond. A* **150**, 166 (1935).
- [61] K. Roberts and S. R. Valluri, *Can. J. Phys.* **95**, 105 (2017).
- [62] H. P. Rojas and E. R. Querts, in *Proc. MG10 Meeting*, edited by M. Novello *et al.* (World Scientific, 2006), p. 2241.
- [63] H. P. Rojas and E. R. Querts, *Int. J. Mod. Phys. D* **16**, 165 (2007).
- [64] J. Schwinger, *Phys. Rev.* **82**, 664 (1951).
- [65] A. E. Shabad and V. V. Usov, *Phys. Rev. D* **83**, 105006 (2011).
- [66] R. Taverna *et al.*, *Mon. Not. R. Astron. Soc.* **454**, 3254 (2015).
- [67] R. Taverna *et al.*, *Science* **378**, 646 (2022).
- [68] W.-y. Tsai and T. Erber, *Phys. Rev. D* **12**, 1132 (1975).
- [69] C. M. Kim and S. P. Kim, arXiv:2202.05477 (2022).
- [70] R. Turolla *et al.*, *Astrophys. J.* **954**, 88 (2023).
- [71] S. R. Valluri, M. Gil, D. Jeffrey, and S. Basu, *J. Math. Phys.* **50**, 102103 (2009).
- [72] S. R. Valluri, D. J. Jeffrey, and R. M. Corless, *Can. J. Phys.* **78**, 823 (2000).
- [73] S. R. Valluri *et al.*, *Mon. Not. R. Astron. Soc.* **472**, 2398 (2017).
- [74] S. Villalba-Chávez and H. Pérez-Rojas, arXiv:hep-th/0609008 (2006).
- [75] S. Villalba-Chávez, *Phys. Rev. D* **81**, 105019 (2010).
- [76] S. Villalba-Chávez and A. E. Shabad, *Phys. Rev. D* **86**, 105040 (2012).
- [77] A. D. Spector, T. Kozłowski, and L. Roberts, arXiv:2510.14064 (2025).
- [78] C. Wang and D. Lai, *Mon. Not. R. Astron. Soc.* **398**, 515 (2009).
- [79] V. Weisskopf, *K. Dan. Vidensk. Selsk. Mat. Fys. Medd.* **14**, 1 (1936).
- [80] S. Zane *et al.*, *Astrophys. J. Lett.* **944**, L27 (2023).
- [81] E. Zavattini *et al.*, *Phys. Rev. D* **77**, 032006 (2008).
- [82] G. Zavattini and E. Calloni, *Eur. Phys. J. C* **62**, 459 (2009).
- [83] P. V. Sasorov, F. Pegoraro, T. Zh. Esirkepov, and S. V. Bulanov, *New J. Phys.* **23**, 105003 (2021).
- [84] P. V. Sasorov and S. V. Bulanov, arXiv:2508.09214 (2025).

## Appendix A: Proof of Positivity and Monotonicity

We prove that

$$\frac{d}{dB}n_{\perp}(B) \geq 0 \quad (\text{A1})$$

and subsequently

$$\frac{d}{dB}\langle H(B) \rangle \leq 0 \quad (\text{A2})$$

for the perpendicular mode.

Using

$$n_{\perp}(B) = 1 + \frac{1}{2}B^2 \left. \frac{\partial^2 \mathcal{L}}{\partial \mathcal{G}^2} \right|_{\mathcal{G}=0}^{\mathcal{F}=B^2/2} \quad (\text{A3})$$

and Eq. (63) of Shabad & Usov [65]:

$$B^2 \left. \frac{\partial^2 \mathcal{L}}{\partial \mathcal{G}^2} \right|_{\mathcal{G}=0}^{\mathcal{F}=B^2/2} = \frac{\alpha}{3\pi} B^2 \frac{1}{2\mathcal{F}} \int_0^{\infty} \frac{dt}{t} \exp\left(\frac{-t}{b}\right) \times \left[ \frac{-3 \coth t}{2t} + \frac{3}{2 \sinh^2 t} + t \coth t \right], \quad (\text{A4})$$

where  $b = B/B_{\text{cr}}$ .

Differentiating the RHS of Eq. (A4) with respect to  $B$ :

$$\frac{\alpha}{3\pi} \int_0^{\infty} \frac{dt}{b^2} \exp\left(\frac{-t}{b}\right) \times \left[ \frac{-3 \coth t}{2t} + \frac{3}{2 \sinh^2 t} + t \coth t \right]. \quad (\text{A5})$$

Noting that

$$\left[ \frac{-3 \coth t}{2t} + \frac{3}{2 \sinh^2 t} + t \coth t \right] \geq 0 \quad (\text{A6})$$

for each  $t > 0$  (verified numerically and analytically) proves Eq. (A1) and subsequently Eq. (A2).

For comparison, the anomalous magnetic moment of an electron is [76]:

$$\mu_{e,\text{anom}} = \frac{\alpha}{2\pi} \frac{1}{2} \frac{e}{m}. \quad (\text{A7})$$

Using  $\mu_{\gamma}(B) \simeq \frac{\alpha}{4\pi} \frac{2}{3} \frac{e}{m}$ :

$$\mu_{\gamma}(B) \simeq \frac{2}{3} \mu_{\text{anom},e^{-}}. \quad (\text{A8})$$

Equation (A8) provides an experimental upper bound for  $\mu_{\gamma}$  in terms of the Bohr magneton [2]:

$$\mu_{\gamma}(B) \sim 7.7 \times 10^{-4} \mu_{\text{Bohr}}. \quad (\text{A9})$$

From  $d\langle H \rangle/dB \leq 0$ :

$$2B\gamma_{\mathcal{G}\mathcal{G}} + B^3\gamma_{\mathcal{F}\mathcal{G}\mathcal{G}} \geq 0, \quad (\text{A10})$$

where

$$\gamma_{\mathcal{F}\mathcal{G}\mathcal{G}} = \left. \frac{\partial^3 \mathcal{L}}{\partial \mathcal{F} \partial \mathcal{G}^2} \right|_{\mathcal{G}=0}^{\mathcal{F}=B^2/2}. \quad (\text{A11})$$

From  $d^2\langle H \rangle/dB^2 \leq 0$ :

$$2\gamma_{\mathcal{G}\mathcal{G}} + 5B^2\gamma_{\mathcal{F}\mathcal{G}\mathcal{G}} + B^4\gamma_{\mathcal{F}\mathcal{F}\mathcal{G}\mathcal{G}} \geq 0, \quad (\text{A12})$$

where

$$\gamma_{\mathcal{F}\mathcal{F}\mathcal{G}\mathcal{G}} = \left. \frac{\partial^4 \mathcal{L}}{\partial \mathcal{F}^2 \partial \mathcal{G}^2} \right|_{\mathcal{G}=0}^{\mathcal{F}=B^2/2}. \quad (\text{A13})$$

### Appendix B: Derivation of Eq. (36)

The starting point is Eq. (12) of Karbstein & Shaisultanov [45]:

$$\left. \frac{\partial^2 \mathcal{L}}{\partial \mathcal{G}^2} \right|_{\mathcal{G}=0} = \frac{1}{2\mathcal{F}} \frac{\alpha}{\pi} \left\{ 4\zeta'(-1, \chi) - \chi[2\zeta'(0, \chi) - \ln(\chi) + \chi] - \frac{1}{3}\psi(\chi) + \chi^{-1} + 1 \right\}, \quad (\text{B1})$$

where

$$\chi = \frac{m^2}{2\sqrt{2|\mathcal{F}|}} \times \begin{cases} 1 & \text{for } \mathcal{F} \geq 0 \\ i & \text{for } \mathcal{F} \leq 0 \end{cases} \quad (\text{B2})$$

For  $\mathcal{F} = B^2/2 \geq 0$  and  $B > 0$ , using

$$\frac{d}{dB} \zeta' \left( -1, \frac{1}{2B} \right) = \frac{-\ln \Gamma \left( \frac{1}{2B} \right) + \frac{1}{2} \ln(2\pi) - \frac{1}{2B} + \frac{1}{2}}{2B^2}, \quad (\text{B3})$$

we obtain:

$$\left. \frac{d}{dB} \left( \frac{1}{2} B^2 \gamma_{\mathcal{G}\mathcal{G}} \right) = \frac{\alpha}{4\pi} \left\{ \frac{2}{3} + \frac{1}{B^3} \left[ \frac{B}{3} \psi' \left( 1 + \frac{1}{2B} \right) + \psi \left( \frac{1}{2B} \right) - 2B \ln \Gamma \left( \frac{1}{2B} \right) + B \ln(2\pi) + \ln(2B) \right] \right\}. \quad (\text{B4})$$

From the relation  $\mu_B = -d\langle H(B) \rangle / dB$ , we obtain Eq. (36).

We use the inequality

$$\psi''(1+h) \leq -\frac{1}{h^2} + \frac{1}{h^3} - \frac{1}{2h^4} + \frac{1}{6h^6}, \quad h > 0, \quad (\text{B5})$$

plus similar inequalities for  $\psi'$ ,  $\psi$ , and  $\ln \Gamma$ .

For  $h = 1/(2B)$ :

$$-\frac{1}{6B^4} \psi''(1+h) \geq -\frac{1}{6B^4} \left( -\frac{1}{h^2} + \frac{1}{h^3} - \frac{1}{2h^4} + \frac{1}{6h^6} \right). \quad (\text{B6})$$

### Appendix C: Proof of Convexity

We establish that

$$\frac{d^2}{dB^2} n_{\perp}(B) \geq 0 \quad (\text{C1})$$

and subsequently

$$\frac{d^2}{dB^2} \langle H(B) \rangle \leq 0. \quad (\text{C2})$$

Using

$$\left. \frac{d^2}{dB^2} \left( \frac{1}{2} B^2 \gamma_{\mathcal{G}\mathcal{G}} \right) = \frac{d}{dB} \frac{\alpha}{4\pi} \left\{ \frac{2}{3} + \frac{1}{B^3} \left[ \frac{B}{3} \psi' \left( 1 + \frac{1}{2B} \right) + \psi \left( \frac{1}{2B} \right) - 2B \ln \Gamma \left( \frac{1}{2B} \right) + B \ln(2\pi) + \ln(2B) \right] \right\} \quad (\text{C3})$$

for  $0.44 \geq B \geq 0$ , we arrive at

$$\frac{d\mu(B)}{dB} \geq \frac{\alpha}{4\pi} \left( \frac{28}{45} - \frac{156}{49} B^2 \right) \frac{|\mathbf{k}|}{m} \sin^2 \theta. \quad (\text{C4})$$

For  $0 \leq B \leq 0.44 B_{\text{cr}}$ :

$$\frac{\alpha}{4\pi} \left( \frac{28}{45} - \frac{156}{49} B^2 \right) > 0. \quad (\text{C5})$$

Since

$$\frac{d^2}{dB^2} \langle H(B) \rangle = -\frac{d\mu(B)}{dB}, \quad (\text{C6})$$

Eq. (C2) is established. Similarly,

$$\frac{d^2}{dB^2} n_{\perp}(B) = -\frac{d\mu(B)}{dB} \cdot \frac{|\mathbf{k}|}{|\mathbf{k}|} > 0. \quad (\text{C7})$$